Nanoscale

Raman Spectroscopy of Bottom-Up Synthesized Graphene Quantum Dots: Size and Structure Dependence

Journal:	*Nanoscale*
Manuscript ID	NR-ART-06-2019-005345.R1
Article Type:	Paper
Date Submitted by the Author:	02-Aug-2019
Complete List of Authors:	Dervishi, Enkeleda ; Los Alamos National Laboratory Ji, Zhiqiang; Los Alamos National Laboratory Htoon, Han; Los Alamos National Lab, MPA-CINT Sykora, Milan; Los Alamos National Laboratory Doorn, Stephen; Los Alamos National Laboratory

Raman Spectroscopy of Bottom-Up Synthesized Graphene Quantum Dots: Size and Structure Dependence

Enkeleda Dervishi,[†] Zhiqiang Ji,[‡] Han Htoon,[†] Milan Sykora,[‡,§] and Stephen K. Doorn[†*]

[†]Materials Physics and Applications Division, Center for Integrated Nanotechnologies, [‡]Chemistry Division, Los Alamos National Laboratory, Los Alamos, New Mexico 87545, United States

[§]Present address: Laboratory for Advanced Materials, Faculty of Natural Sciences, Comenius University, 84215 Bratislava, Slovakia

ABSTRACT:

Graphene quantum dots (GQDs) have attracted significant interest as synthetically tunable optoelectronic and photonic materials that can also serve as model systems for understanding size-dependent behaviors of related graphene structures such as nanoribbons. We present a Raman spectroscopy study of bottom-up synthesized GQDs with lateral dimensions between 0.97 to 1.62 nm, well-defined (armchair) edge type, and fully benzenoid structures. For a better understanding of observed size-dependent trends, the study is extended to larger graphene structures including nano-graphene platelets (>25 nm) and large-area graphene. Raman spectra of GQDs reveal the presence of D and G bands, as well as higher order modes (2D, D+G, and 2G). The D and G band frequencies and intensity were found to increase as GQD size increases, while higher order modes (2D, D+G, and 2G) also increased in intensity and became more well-defined. The integrated intensity ratios of D and G bands (I_D/I_G) increase as the size of the GQDs approaches 2 nm and rapidly decrease for larger graphene structures. We present a quantitative comparison of I_D/I_G ratios for the GQDs and for defects introduced into large area graphenes through ion bombardment, for which inter-defect distances are comparable to the sizes of GQDs studied here. Close agreement suggests the I_D/I_G ratio as a size diagnostic for other nanographenes. Finally, we show that Raman spectroscopy is also a good diagnostic tool for monitoring the formation of bottom-up synthesized GQDs.

*email: skdoorn@lanl.gov

KEYWORDS: graphene quantum dot, graphene molecule, nanographene, Raman spectroscopy, nanocarbon

Introduction

Graphene quantum dots (GQDs), nanometer-sized fragments of graphene, have size and structurally tunable optical and electronic properties[1,2] that make them promising materials for a wide range of applications, including photovoltaics,[3-6] electrochromics,[7] light-emission,[8-12] memory devices,[13] and bio-sensing.[14-17] GQDs are generally produced via top-down chemical/thermal break down of larger graphitic structures using acidic exfoliation, ion-bombardment (irradiation via e-beam or x-rays), microwave /UV irradiation, etc.,[18-20] or by bottom-up solution-based chemical synthesis.[3-5,21,22] Bottom-up synthetic approaches have the advantage of reproducibly generating ensembles of well-defined GQD structures. [3-5,21,22] The type and concentration of defects and functional groups present in the graphene structure are strongly dependent on the preparation method and post-preparation processing.[4,5,21-24]

Due to their nanometer size, GQDs serve as model systems for studying how graphene properties transform as size approaches the molecular limit. In this regard they are important structures for understanding extremes of graphene behavior and properties of other planar nanocarbons, such as graphene nanoribbons. In addition to such fundamental considerations, growing interest in applications requires accurate and rapid characterization of synthesis intermediates as well as final materials. Characterization must be sensitive to morphological features, such as size, edge-type and defect concentration, which strongly affect their electronic, optical and mechanical properties.[19,25,26] In previous studies, GQD characterization has included use of NMR, FTIR, STM, AFM, HRTEM, XPS, and MALDI-TOF-MS, which can be either time consuming, complex, require a large amount of test sample or are not sufficiently sensitive to specific GQD features.[5-7,10,26-28]

As a complementary technique, Raman spectroscopy is rapid, non-destructive, and capable of probing a wide variety of graphitic materials to characterize doping level, crystallite size, number of layers, edge-type, chemical functionality, and presence/type of defects.[24,27-35] Of specific interest is the evolution of position and intensity of two dominant spectral bands, the disorder-induced D band and the G band, which have been effectively used to identify and quantify defect concentration in various graphitic materials.[23,27-34]

Raman studies have been performed previously to understand the size-dependent nature of defects on ion-bombarded graphene structures with inter-defect distances ranging from ~1-24 nm.[30,32] The resultant defect structures, however, are poorly defined. Furthermore, it remains to be shown if the trends in their size dependence may be used to model expectations for graphene crystallites, whose size-dependent spectra have been probed systematically only to dimensions on the order of 5-10 nm.[24,28,33]

GQDs provide a well-defined system for extending our knowledge of disorder and size-dependent behavior in graphene to the smallest length scales. However, to the best of our knowledge, the size-dependent properties of well-defined GQD structures generated from bottom-up synthesis have not yet been systematically studied by Raman spectroscopy. Here we perform a systematic Raman spectroscopy study of GQDs prepared by bottom-up, surface-assisted synthesis,[3,7] producing reproducible materials with well-known structure and size. We examine Raman spectra of a series of GQDs with armchair edges and fully benzenoid structures, with controlled lateral dimensions (L) varying between 0.97 nm and 1.62 nm. We study the evolution of the intensity ratios of D and G modes, as well as their respective spectral positions, with GQD size. The understanding of the variation in the Raman spectral features with size in GQDs smaller than 2nm fills an important knowledge gap. In agreement with previous work on top-down generated defects,[30,32] for the synthesized GQDs we find that, at the smallest length scales, D/G intensity ratio increases with GQD size, up to a ~2 nm limit. For structures larger than 2 nm, D/G intensity ratio decreases, as the size continues to increase. Finally, we also use Raman spectroscopy to probe how specific spectral features evolve as the GQD forms during chemical synthesis. Evolution of the spectra during the formation of the GQDs provides insight into the reaction mechanism and establishes Raman as an effective tool for mechanistic studies of formation of nanometer-sized graphene structures.

Results and Discussion

GQD Raman Spectroscopy

We studied three GQD structures (Figure 1a) of increasing dimension ranging from 0.97 nm to 1.62 nm (see Supporting Information Figure S1 and Table S1), with chemical compositions $C_{60}H_{23}(COOH)$, $C_{132}H_{36}(COOH)_2$, and $C_{204}H_{48}(COOH)_2$. To simplify further

discussion, the GQDs are labeled GQD(1), GQD(2), and GQD(3), respectively. All three GQDs were synthesized on the surface of nanocrystalline titanium dioxide (*nc*-TiO_2) films (see Scheme 1 and Methods), following the procedures described in detail in our previous work.[2] All synthesized structures are fully benzenoid with 6n π conjugated electrons, where n = 60, 132, and 204 (with number of conjugated rings N_{CR} = 19, 48 and 79, respectively), which means that no zero energy edge states are present in any of the structures.[2,36] Figure 1b shows UV-Vis-near-IR absorption spectra of all three GQDs studied here. The dominant absorption bands red-shift with increasing GQD size, which is a result of quantum confinement on their electronic structure.[2] Figure 1b also shows the excitation wavelengths used in the Raman studies (532 nm and 405 nm) superimposed on the absorbance spectra. We obtained Raman spectral response for all three GQDs at both excitation wavelengths.

Raman spectra of the GQDs in the spectral range 900-3300 cm^{-1} are shown in Figure 2 (532 nm exc.) and Figure S2 (405 nm exc.). The spectra show typical graphitic features including the D mode (~1315-1335 cm^{-1}), activated by symmetry breaking at defects and edges,[34] the G-band (~1595 cm^{-1}), which arises due to in-plane C-C deformations,[34] and second order features corresponding to 2D, D+G, and 2G combination modes/overtones. Interestingly, although the GQDs studied here approach molecular sizes, all three systems yielded spectra highly characteristic of extended graphene structures. For all GQDs the observed spectra were independent of the measurement position on the sample (see Figure S3), indicating that the syntheses were homogeneous across the surface of the TiO_2 films, independent of the GQD size. No fluorescence background was apparent in the Raman spectra, likely as a result of the GQDs being adsorbed to the TiO_2 film.

We observe size-dependent trends in both D and G-band frequencies, with each decreasing as GQD size increases (G decreasing from 1597 to 1594 cm^{-1} and D decreasing from 1335 to 1315 cm^{-1}, see Figure 3). These observations are consistent with the trends found in large-area graphenes, for which defects were intentionally introduced using argon-ion bombardment.[23,31] In the latter case, as defect size and density decrease (effectively translating to larger crystallite size in nanographenes), D and G-band frequency also decrease.[23,31] D-band behavior in both systems can be attributed to quantum confinement effects as they relate to the dispersive second-order double-resonance nature of Raman scattering for this mode.[34] The D-mode process involves optical excitation followed by two intervalley scattering events within the graphene Brillouin zone for the electron (or hole),

each involving either a D phonon or a defect.[34] The size dependence we observe for GQDs is similar to that observed for D-mode scattering in carbon nanotubes. In the latter, as diameter increases, both transition energy and resonant phonon wave vector decrease.[37] Thus for larger-diameter nanotubes this mode is observed at lower frequency.[37,38]

While the dependence of the G-mode frequency on GQD size follows qualitatively the same trend, the effect is significantly smaller. We attribute this to the fact that the G-mode has its origin in a first-order scattering process that is not affected by quantum confinement effects. Instead, the G-mode size dependence is likely increasingly influenced by edge effects for the smaller structures. As GQD size decreases, the H/C ratio increases (see Figure 1a), which may have the effect of mixing in contributions from the higher frequency (~3000 cm^{-1}) C-H vibrations. G frequency for the larger GQDs trends towards that observed for graphene (1580 cm^{-1}), for which the continuous sp^2 conjugated lattice reduces strain.

The size-dependent changes in D-mode frequencies show significant dependence on the excitation wavelength. With 405 nm excitation (Figure 3a), only a minor decrease in D frequency is observed as GQD size increases. In contrast, the effect is much more dramatic for 532 nm excitation. The smaller size dependence observed for 405 nm excitation suggests that quantum confinement is less significant for higher energy excitations and is likely a further consequence of the dispersive nature of this mode. At higher energy excitations it is possible to access regions of the band structure that are no longer parabolic in nature and have significantly reduced curvature, such as that exhibited near the M-point.[34] The shallower potential surface will by its nature display weaker dispersion with excitation energy, thus providing a basis for the reduced sensitivity of the D-mode to GQD size. With the G-mode being non-dispersive and first-order in nature, it is expected to show no dependence on excitation energy, in agreement with our observations (see Figure 3b).

D to G Mode Intensity Ratios

In addition to the D and G mode frequencies, the relative intensities of these modes are another important characteristic of the graphene structures. Specifically, the I_D/I_G ratio (where I_D and I_G are the integrated D and G band intensities, respectively) is an important figure of merit related to the defect density and the crystallite size.[34] Jorio and co-workers precisely quantified how the I_D/I_G ratio varies with defect density by introducing defects into

graphene via exposure to controlled levels of Ar-ion bombardment, which creates localized regions of disorder in the normally hexagonal graphene lattice.[27-32] Average inter-defect spacings (L_D) ranging from 1 nm to 24 nm were produced in this way. Opposing trends in the I_D/I_G ratio were observed at two distinct length scales. As defect density increased from the limit of pristine graphene (no defects) to that with L_D values of 3 nm, the I_D/I_G ratio was found to increase as well. Beyond this limit, as defect densities continued to increase (corresponding to a further decrease in L_D values from 3 nm to 1 nm) the I_D/I_G ratio was found to decrease.[27-32] Thus, a peak in the I_D/I_G vs. L_D curve was observed at an L_D of ~3 nm.[30,32]

This behavior was rationalized by considering expectations for trends in D and G-band intensity across the two regimes of defect-density. Because the D-band is activated by the presence of defects,[34] its intensity must increase as defect density initially increases (*i.e.*, as L_D decreases from 24 nm to 3 nm). At the smallest inter-defect spacings (*i.e.*, as L_D decreases from 3 nm to 1 nm), however, disordered regions overlap and the graphene lattice becomes progressively more disrupted.[30,32] L_D in this regime becomes less than the coherence length (~ 3 nm)[30,32] of electrons before scattering by a phonon occurs.[30,32] As a result, contributions from individual defects do not independently sum, acting to decrease D-band intensity as L_D decreases. Additionally, because the D mode is a breathing mode of 6-atom rings,[32,34] as the graphene hexagonal structure breaks up at high defect densities, the D band loses intensity.[32] In contrast, since the G-band intensity arises from relative motion of sp^2 carbons, G intensity remains relatively constant across the full range of inter-defect distances.[32] The combined D and G-band intensity behaviors thus explain the peak in the I_D/I_G ratio as L_D changes.

There is debate on whether a similar trend should also exist for graphene nanocrystallites as their size decreases below that of the Raman relaxation length discussed above.[32] With the edge of a graphene nanocrystallite serving as a symmetry-breaking defect, a similar I_D/I_G response might be expected in relation to crystallite size. However, as crystallite size decreases, both numbers of sp^2 carbons (n) and six-member rings (N_{CR}) will decrease, presenting a qualitative difference between the factors determining D and G-band intensities, in comparison to those underlying Raman response in disordered large-area graphene. Evaluation of the I_D/I_G response for crystallite sizes less than 5 nm (*i.e.,* smaller than the Raman coherence limit) is required to answer this question, but such a study has not

yet been reported.[24,28,33] The GQD series investigated here provides an opportunity to address this deficiency.

In Figure 4 we show a plot of the I_D/I_G ratio as a function of the number of conjugated carbons, n, and the number of ordered rings, N_{CR} (panel 4a), and as a function of GQD lateral size, L, (panel 4b) for GQDs(1-3). The values of L were determined as the average of the lateral distances across the short axis of each GQD. As n and N_{CR} increase, we find I_D/I_G (obtained with 532 nm excitation) to also increase (Figure 4a). Similarly, I_D/I_G is also found to increase as the inter-edge distance, L, increases (Figure 4b). This parallels the observed behavior of the intentionally defected graphene, for which at the smallest inter-defect spacings, as L_D increases, so too do D-band intensity and the I_D/I_G ratio.[27-32]

The parallel in I_D/I_G behaviors is significant because its origin in GQDs is somewhat different than for the intentionally disordered graphene. In the disordered graphene, as L_D changes at the smallest length scales, N_{CR} changes in the same direction. The number of sp^2 carbons (n), however, remains relatively constant.[32] In contrast, for the GQDs all three size-related parameters (L, n, N_{CR}) change in the same direction. Our GQD results are suggestive that the effects of increasing n (translating to an increase in G-band intensity) and those of increasing N_{CR} (translating to an increased D-band intensity) effectively cancel. Our observation of an increase in I_D/I_G as GQD size increases suggests instead that the ultimate factor in determining the GQD I_D/I_G behavior is L and its relation to the Raman coherence length of the D mode.

Despite the somewhat different origins, we find that the variation in the I_D/I_G ratio with L observed here for the GQDs agrees well (see Figure 4b) with the relation established by Jorio and co-workers[30,32] for large-area graphenes with introduced defects. For Ar^+ irradiated graphene, the relation between I_D/I_G and L_D is quantified as the sum of contributions from an activated region within the coherence length of the induced defect and from the disordered region itself,[30,32] as per eq. 1:

$$\frac{I_D}{I_G} = C_A f_A + C_S f_S \qquad (1)$$

In eq. 1, f_A is the fractional activated area, while f_S is the fractional disordered area of the defects themselves, with C_A and C_S being the respective scaling coefficients (see additional

details in Supporting Information). Ref. 30 assumes contributions from both regions, while Ref. 32 neglects the second term, under the assumption that disordered regions are too disrupted structurally to generate D-band intensity.[32] This exclusion is accommodated by an increase in the C_A value (see Supporting Information). We plot both forms in comparison to our GQD data in Figure 4b. To extend the comparison to graphene materials of larger dimension and confirm that the trend observed here for small GQDs(1-3) reverses for larger values of L, we add to the figure I_D/I_G values obtained for nano-graphene platelets (L ~25 nm) grown via a bimetallic FeMoMgO catalytic growth process and also for large area graphene grown on copper foil (see Methods and also Figures S4 and S5 for representative Raman spectra of the platelets and large area graphene). The results in Figure 4b show that these larger area graphenes map to the expected region in which I_D/I_G decreases as defect density decreases.

Interestingly, we find that both terms in eq. 1 must be used to quantitatively describe the I_D/I_G response with L for the GQDs. Neglecting response from the disorder term (black curve, Figure 4b) significantly underestimates the I_D/I_G value, relative to the experimentally measured GQD results. In contrast, use of both terms of eq. 1 (blue curve, Figure 4b) yields close agreement between the model and experiment. This result indicates that the I_D/I_G response in GQDs effectively acts as a superposition of activated and disordered region behaviors. Furthermore, while the disordered region is located at the core of the induced defects, the corresponding values of L for GQDs encompass the entire GQD structure and thus must be considered as contributing to the D-band intensity. Thus, inclusion of both terms is essential for capturing all sources of D-band intensity in the GQDs. The results shown in Figure 4 thus provide a direct link between the behavior of crystallite size and inter-defect distance over the entire inter-defect distance range probed previously.[27-32] While the nature of the defects in large-area graphene and the GQD edge defects are fundamentally different, they ultimately follow similar trends.

The agreement of the GQD I_D/I_G behavior with the model of Jorio and co-workers[30,32] indicates that measurement of I_D/I_G values has potential for use in evaluating length scales of other nanographenes, such as graphene nanoribbons and other GQD types. Because of the peaked nature of the plot of I_D/I_G vs. defect length-scale, however, ambiguity exists in the result, since one value of I_D/I_G could correspond to two different values of the length scale. This ambiguity can be removed by considering the linewidth of the D and G bands. It has

been shown previously that both the D and G-band linewidths remain nearly constant (at values effectively represented by those found for typical large-area graphenes, i.e. ~20 (D) and 15 (G) cm^{-1} full-width at half-max, FWHM) for the low defect-density side of the I_D/I_G curve.[23,29,31,32] On the high defect-density side, however, the linewidths are found to steadily increase with defect density. [23,29,31,32] The D and G-band linewidths are thus ready indicators of which side of the curve a particular I_D/I_G response exists. Similar behavior is found for the D and G-band linewidths in the GQDs. As GQD size decreases, linewidths increase significantly (see Figure 5). On going from GQD(3) to GQD(1), linewidth for the D band increases from 70 to 110

cm^{-1} FWHM, while that for the G band increases from 30 to 43 cm^{-1}. In contrast, linewidths for the D and G-band in our large-area graphene sample is similar to those previously reported: 25 and 17 cm^{-1} FWHM, respectively (Figure S5a). The linewidth comparison is consistent with the expectation that the I_D/I_G values for the GQDs lie on the high defect-density side of the length-scale curve (Figure 4b) and supports the use of linewidth as a means for lifting ambiguity in evaluating defect length scale using I_D/I_G values.

It is important to note that D-band scattering is not activated by zigzag edge structure,[39,40] complicating interpretation of results on systems without synthetic control of edge structure. For example, the ion-bombardment based techniques were found to generate graphitic structures with an irregular shape and undefined edges.[30] The GQD edge structure, however, is exclusively armchair, which makes these nanostructures important reference points as systems for systematic studies of the size-dependent trends in graphene. One observation directly related to nature of the edge structure is that our I_D/I_G results for GQDs lie consistently above those of the Jorio analysis (Figure 4b).[30] Because the GQDs have fully armchair edge structures, we expect to observe the maximum theoretical D-band intensity for these systems. In contrast, the poorly defined edge structures of the ion-bombarded graphene, which presumably also contain a mix of zigzag edges, are expected to display weaker D-mode intensity.

Somewhat different trends are observed for I_D/I_G ratios obtained using 405 nm excitation. As seen in Figures 4a and b, the overall magnitude of the ratio is significantly smaller for 405 nm excitation compared to that obtained with 532 nm excitation. This is in line with the inverse E^4 dependence in excitation energy (E) established for I_D/I_G by Cancado et al.[32] Such a dependence will tend to flatten the trend with respect to crystallite size and L.

We indeed observe a relatively flat dependence on size and L. The excitation energy dependence is ultimately related to the band dispersion and is dependent on how scattering efficiency changes between the K and Γ points of the graphene Brillouin zone.[32] As we found with the D-band frequency, the flatness of the results of Figure 4a and b is further suggestive of 405 nm excitation probing a flatter (lower dispersion) region of the band structure for GQDs.

Anomalous and Second-Order Raman Features

Close inspection of the Raman spectra shown in Fig.2 reveals that the D band shows a pronounced asymmetry, with a shoulder (labeled D*) appearing at lower frequency for 532 nm excitation and higher frequency for 405 nm excitation (see Figure S2). Additionally, a broad region of increased intensity appears between the D and G bands. Such features are not observed in large area graphenes and large area nanocrystallites, which show symmetric D bands (e.g., see Figures S4 and S5). Interestingly, ion bombardment of graphene also does not induce such asymmetry,[30-32] which indicates that the spectral feature does not have its origin in physical defects or material edges. Similar features, however, were observed in Raman spectra of graphene oxide and for exfoliated graphene flakes that have been oxidized.[24,35,41] Such behavior can arise from oxygen functionality bound to the interior of the graphene structure, as well as at graphene edges.[24,35,41] It is therefore likely, that the asymmetric D-band feature observed in the Raman spectra of the GQDs studied here arises from the carboxylate functionality present in each of our GQD structures.

While our discussion has focused on the D and G band behavior, we note that GQD size also impacts the higher frequency second-order modes (2D, D+G, and 2G) observed at 2614, 2905, and 3187 cm^{-1}, respectively (Figures 2 and S2). As we go across the series from GQD(1) to GQD(3), these higher-order modes become more intense and better defined. As size is further increased to include the 25 nm platelets and large area graphenes, the 2D mode is found to increase significantly, to the point of dominating the Raman spectrum, while the D+G and 2G modes disappear (see Figures S4 and S5). These trends again closely mirror those introduced by ion-bombardment of pristine graphene.[23,30,31] The higher-order modes are thus another indicator of the connection between the edge-induced scattering in the smallest graphene crystallites and defect-induced behaviors in more monolithic materials.

It is interesting to note the absence of the D' band in the GQD spectra. This phonon, appearing at slightly higher frequencies than the G band, is an intravalley scattering analogue of the D band and is also activated by defects.[34] In graphene systems with point defects, the D' mode grows in intensity as defect density increases.[23,31,32] The absence of this band in GQDs is an interesting contrast to the behavior arising from point defects and highlights an important difference between the two types of defect-based symmetry breaking. While the D' band is allowed by symmetry for both zigzag and armchair edge structures, its intensity may be determined by other factors that are not yet well-understood.[32,34] Considering edge structures as an origin for this mode, it has been observed for large-area graphene edges[42] and in certain graphene nanoribbons,[43] but not for systems (large-area or nanoribbon) in which the edges have been well-characterized as armchair.[42,44-47] Such a lack of the D' mode for armchair edges suggests that our all-armchair GQDs will exhibit a similar response.

Raman as a Diagnostic Probe of GQD Synthesis

The sensitivity of D, G, and higher-order modes to the structure of the GQDs makes Raman spectroscopy a useful diagnostic tool for following the progress of the GQD syntheses. Evolution of these modes can act as an indicator of the reaction progress in the final conversion step from the non-conjugated precursor to the fully conjugated GQD. As shown in Figure S1, the GQD precursors (composed of dendrimer-like assemblies of phenyl rings) must be subjected to an anaerobic conjugation step (typically 1 hour in duration) to fully chemically couple the phenyl rings (Scheme 1). To probe the progress of this conjugation step, we obtained Raman spectra (see Figure 6a-c) of the reaction system at t = 0 seconds (starting material, Figure 6a), 30 seconds, 5 minutes, and 1 hour. Inspection of the high-frequency region of the spectrum shows that as the reaction progresses, the higher-order 2D, D+G, and 2G modes become more intense and better defined, indicating that the GQD structure is becoming more ordered as the reaction progresses. Additionally, both D and G mode frequencies decrease (Figure 6d) and the I_D/I_G ratio increases with reaction time (Figure 6e). This behavior was observed for GQD(3), as well as for GQD(2).

As discussed earlier, spectral evolution reflects the nature and extent of the sp^2 network as it is being formed in the last step of the GQD synthesis. Because the precursor system is not fully conjugated, it lacks the higher order features of the GQDs and also displays minimal D band intensity (Figure 6a). As the reaction progresses, formation of the

sp^2 network and benzenoid ring structures takes place, as reflected in the higher order and D and G mode spectral response. In fact, the spectrum at 30 seconds indicates significant conjugation of the network shortly after initiation of the conjugation reaction. We find the spectra to remain virtually unchanged after 5 minutes, indicating that the reaction is already nearly complete at this time. Raman probing of the reaction progress thus provides information about the rate of formation of the sp^2 network, demonstrating its utility as a reaction diagnostic for development of these and related types of nanocarbon materials.

Conclusions

We have presented a systematic analysis of the effect of size on Raman spectra for a series of bottom-up synthesized GQDs, with sizes 0.89 – 1.62 nm, and compared the results with spectra of larger-scale (> 20 nm) graphene nanoplatelets[48] and large-area graphenes. We find that even in such small GQD structures, the spectra are dominated by the D and G Raman bands, whose frequencies increase with decrease in GQD size, consistent with quantum confinement effects.[2] Additionally, higher-order modes become better defined as GQD size increases and their sp^2 networks become more extensive.

Of particular importance is the ratio I_D/I_G as a measure of defect density, for which GQD edges mimic defect sites in larger area graphenes. Our results show that variation of the I_D/I_G ratio with GQD size is in good agreement with the prior studies of highly defected large area graphenes,[30,32] for which defect separation distances exist in the same length scales as our GQD sizes. The close quantitative agreement between the two studies demonstrates that such analysis can be used as a quantitative basis for understanding and predicting behaviors of nanographenes from large area structures down to the smallest dimensions. This observation could be particularly helpful in studies of graphene nanoribbons. Nanoribbons are expected to display a radial breathing-like (RBLM) mode in their Raman spectra, whose frequency is directly dependent on the ribbon width.[49] However, the resonant excitation conditions required to make the RBLM observable may not always be easy to achieve. Measurement of I_D/I_G may provide an alternative route to characterization of nanoribbon widths. Notably, the results we present are for well-defined fully armchair edges.

Such character removes complication introduced by the presence of non-armchair edges, which ultimately may reduce D-band intensities.

Finally, we have shown that GQD spectra evolve from that of their precursors during their synthesis, indicating that Raman spectroscopy may be an effective diagnostic tool in studies of the mechanism and dynamics of GQD formation. Our results highlight the importance of higher-order Raman modes as a signature for evaluating the evolving structural changes during synthesis. In addition to its utility for monitoring GQD growth, Raman will also be a useful tool for following the bottom-up growth from molecular precursors of graphene nanoribbons[50] and other well-defined nanocarbon structures.

Methods

Graphene quantum dots with armchair edges and controlled lateral dimensions smaller than 2 nm were synthesized as described in our previous work.[3,7] Briefly, the respective polyphenylene precursors were synthesized via standard solution-based methods. After pre-adsorbing the precursors on a TiO_2 surface, *in-situ* oxidation using a $FeCl_3$ solution in dichloromethane (Scholl process) was performed to generate the fully conjugated GQDs.[5,7] The chemical structure of the GQDs was confirmed by MALDI-MS. The chemical structures of the precursors and corresponding GQDs are shown in Figure S1. We estimate GQD surface density using a modified Beer's law: $\Gamma(mol/cm^2) = A(\lambda)/1000(cm^3/L)*\varepsilon(\lambda)(M^{-1}cm^{-1})$, where Γ is surface coverage, $A(\lambda)$ is the measured absorbance of the nanocrystalline film and $\varepsilon(\lambda)$ is molar extinction coefficient of the adsorbed molecules, at wavelength λ. We use $\varepsilon(500) \sim 1\times10^5$ M^{-1} cm^{-1} for similar GQD/TiO_2 complexes prepared previously in solution,[22] yielding for GQD(2) an estimate of $\Gamma \sim 2.5\times10^{-9}$ mol/cm^2. This surface coverage is similar to the full surface coverage ($\sim 1\times10^{-8}$ mol/cm^2) of ruthenium polypiridine complexes on TiO_2,[51] suggesting a monolayer coverage by our GQDs and thus limiting any aggregation. The orientation of GQDs on the surface, which can be a factor in the probability of aggregation, is however unknown. Although some aggregation of GQDs is possible, we expect it also to be limited due to the restricted mobility of the GQDs, which are bound to the TiO_2 surface *via* the -COOH anchoring group. Even in the case of some aggregation, previous work on defect effects on mono-, bi-, and trilayer graphene Raman spectra indicates aggregation may have minimum effects on the observed spectra.[31] Assuming sampling of a GQD monolayer in our

measurement, using an excitation spot of 2 μm diameter (see Raman details below), on the order of 10^5 to 10^6 molecules are sampled.

Large-area graphene was synthesized over Cu foil via chemical vapor deposition (CVD). The Cu foil was first treated overnight in acetic acid and subsequently placed in the CVD system. The foil was heated up to 950 °C under an Argon/Hydrogen mixture at 200 sccm for 90 minutes. Next, the furnace temperature was raised to 1020 °C and methane was introduced at 15 sccm for 20 min, at a total pressure of 10 Torr. Finally, the sample was rapidly cooled under Argon/Hydrogen, and transferred to a Si/SiO_2 substrate via a PMMA-assisted technique as previously described.[52]

Nano-graphene platelets were synthesized over a bimetallic catalyst system (FeMoMgO) via chemical vapor deposition.[48] The catalyst was first exposed to Argon at 200 ml/min at 1000 °C. Next, methane was introduced at 30 ml/min for 5 min. Finally, the sample was cooled under Argon and purified using a HCl: H_2O (1:1 ratio) mixture followed by a bath sonication in a H_2SO_4: HNO_3 (3:1 ratio) solution.

Raman measurements were taken using a microscope system with laser excitation wavelengths of 405 nm and 532 nm. The laser was focused onto the sample through an objective (50X, NA = 0.45). Raman signal was collected in an epifluorescence configuration through the same objective and dispersed in a triple monochromator onto a liquid nitrogen-cooled CCD detector (Princeton Instruments). Laser power was kept at 2 mW to prevent heating or damaging the samples. Spectra were obtained using 2 min. integration times and were collected from several areas on the graphene samples in order to assess the homogeneity of these structures. Spectra remained the same over the course of the integration time and for different sampling locations, indicating stability and spatial uniformity of the GQD samples.

ASSOCIATED CONTENT

*S Supporting Information

The Supporting Information is available free of charge on the ACS Publications website at: xxxxxx.

Tabulation of GQD size parameters, GQD precursor and final structures, and additional Raman spectra.

ACKNOWLEDGMENTS

The authors acknowledge financial support from the Los Alamos National Laboratory Directed Research and Development (LDRD) program. E.D. acknowledges funding from the Marie Curie Distinguished Postdoctoral Fellowship at the Los Alamos National Laboratory. This work was performed in part at the Center for Integrated Nanotechnologies, a U.S. Department of Energy Office of Science user facility operated by Los Alamos National Laboratory (Contract DE-AC52-06NA25396) and Sandia National Laboratories (Contract DE-NA-0003525).

References

1. Guclu, A. D.; Potasz, P.; Korkusinski, M.; Hawrylak, P. *Graphene Quantum Dots*. Springer-Verlag: Berlin, 2014.

2. Ji, Z.; Dervishi, E.; Doorn, S. K.; Sykora, M. Size-Dependent Electronic Properties of Uniform Ensembles of Strongly Confined Graphene Quantum Dots. *J. Phys. Chem. Lett*. **2019**, *10*, 953-959.

3. Ji, A.; Wu,R.; Adamska, L.; Velizhanin, K. A.; Doorn, S. K.; Sykora, M. In Situ Synthesis of Graphene Molecules on TiO2: Application in Sensitized Solar Cells. *ACS Appl. Mater. Interfaces* **2014**, *6*, 20473-20478.

4. Yan, X.; Li, B.; Li, L.-S. Colloidal Graphene Quantum Dots with Well-Defined Structures. *Acc. Chem. Res.* **2012**, *46*, 2254−2262.

5. Yan, X.; Cui, X.; Li, B.; Li, L. Large, Solution-Processable Graphene Quantum Dots as Light Absorbers for Photovoltaics. *Nano Lett.* **2010**, *10*, 1869-1873.

6. Kang, S. J.; Ahn, S.; Kim, J. B.; Schenck, C.; Hiszpanski, A. M.; Oh, S.; Schiros, T.; Loo, Y.-L.; Nuckolls, C. Using Self-Organization to Control Morphology in Molecular Photovoltaics. *J. Am. Chem. Soc.* **2013**, *135*, 2207−2212.

7. Ji, Z.; Doorn, S. K.; Sykora, M. Electrochromic Graphene Molecules. *ACS Nano* **2015**, *9*, 4043-4049.

8. Zhang, X.; Zhang, Y.; Wang, Y.; Kalytchuk, S.; Kershaw, S. V.; Wang, Y.; Wang, P.; Zhang, T.; Zhao, Y.; Zhang, H.; Cui, T.; Wang, Y.; Zhao, J.; Yu, W. W.; Rogach, A. L.

Color-Switchable Electroluminescence of Carbon Dot Light-Emitting Diodes. *ACS Nano* **2013**, *7*, 11234–11241.

9. Jin, S. H.; Kim, D. H.; Jun, G. H.; Hong, S. H.; Jeon, S. Tuning the Photoluminescence of Graphene Quantum Dots through the Charge Transfer Effect of Functional Groups. *ACS Nano* **2013**, *7*, 1239-1245.

10. Tetsuka, H.; Asahi, R.; Nagoya, A.; Okamoto, K.; Tajima, I.; Ohta, R.; Okamoto, A. Optically Tunable Amino-Functionalized Graphene Quantum Dots. *Adv. Mater.* **2012**, *24*, 5333-5338.

11. Wang, C.-F.; Yu, Z.-Y.; Guo, X.; Chen, L.; Zhen, S. Facile Access to Versatile Fluorescent Carbon Dots toward Light-Emitting Diodes. *Chem. Comm.* **2012**, *48*, 2692-2694.

12. Zhao, S.; et al. Single Photon Emission from Graphene Quantum Dots at Room Temperature. *Nat. Comm.* **2018**, *9*, 3470.

13. Joo, S. S.; Kim, J.; Kang, S. S.; Kim, S.; Choi, S.; Won, S. Graphene-Quantum-Dot Nonvolatile Charge Trap Flash Memories. *Nanotechnology* **2014**, *25*, 255203.

14. Peng, J.; et al. Graphene Quantum Dots Derived from Carbon Fibers. *Nano Lett.* **2012**, *12*, 844-849.

15. Razmin, H.; Mohammad-Rezaei, R. Graphene Quantum Dots as a New Substrate for Immobilization and Direct Electrochemistry of Glucose Oxidase: Application to Sensitive Glucose Determination. *Biosens. Bioelectron.* **2013**, *41*, 498-504.

16. Esteves da Silva, J. C. G.; Goncalves, H. M. R. Analytical and Bioanalytical Applications of Carbon Dots. *Trends Anal. Chem.* **2011**, *30*, 1327-1336.

17. San, H.; Wu, L.; Wei, W.; Qu, X. Recent Advances in Graphene Quantum Dots for Sensing. *Mater. Today* **2013**, *16*, 433-442.

18. Pan, D.; Zhang, J.; Li, Z.; Wu, M. Hydrothermal Route for Cutting Graphene Sheets into Blue-Luminescent Graphene Quantum Dots. *Adv. Mater.* **2010**, *22*, 734-738.

19. Li, L.; Wu, G.; Yang, G.; Peng, J.; Zhao, J.; Zhu, J. J. Focusing on Luminescent Graphene Quantum Dots: Current Status and Future Perspectives. *Nanoscale* **2013**, *5*, 4015-4039.

20. Zhou, X.; Zhang, Y.; Wang, C.; Wu, X.; Yang, Y.; Zheng, B.; Wu, H.; Guo, Sh.; Zhang, J. Photo-Fenton Reaction of Graphene Oxide: A New Strategy to Prepare Graphene Quantum Dots for DNA Cleavage. *ACS Nano* **2012**, *6*, 6592–6599.

21. Chen, L.; Hernandez, Y.; Feng, X.; Mullen, K. From Nanographene and Graphene Nanoribbons to Graphene Sheets: Chemical Synthesis. *Angew. Chem., Int. Ed.* **2012**, *51*, 7640-7654.

22. Yan, X.; Cui, X.; Li, L. Synthesis of Large, Stable Colloidal Graphene Quantum Dots with Tunable Size. *J. Am. Chem. Soc.* **2010**, *132*, 5944–5945.

23. Eckmann, A.; Felten, A.; Verzhbitskiy, I.; Davey, R.; Casiraghi, C. Raman Study on Defective Graphene: Effect of the Excitation Energy, Type, and Amount of Defects. *Phys. Rev B* **2013**, *88*, 035426.

24. Rajender, G.; Giri, P. K. Formation Mechanism of Graphene Quantum Dots and Their Edge State Conversion Probed by Photoluminescence and Raman Spectroscopy. *J. Mat. Chem. C* **2016**, *4*, 10852-10865.

25. Ritter, K. A.; Lyding, J. W. The Influence of Edge Structure on the Electronic Properties of Graphene Quantum Dots and Nanoribbons", *Nat. Mater.* **2009**, *8*, 235-242.

26. Simpson, Ch. D.; Mattersteig, G.; Martin, K.; Gherghel, L.; Bauer, R. E.; Rader, H. J.; Mullen, K. Nanosized Molecular Propellers by Cyclodehydrogenation of Polyphenylene Dendrimers. *J. Am. Chem. Soc.* **2004**, *126*, 3139-3147.

27. Jorio, A.; Lucchese, M. M.; Stavale, F.; Achete, C. A. Raman Spectroscopy Study of Ar+ Bombardment in Highly Oriented Pyrolytic Graphite. *Phys. Stat. Sol. B* **2009**, *246*, 2689-2692.

28. Cancado, L. G.; Takai, K.; Enoki, T.; Endo, M.; Kim, Y. A.; Mizusaki, H.; Jorio, A.; Coelho, L. N.; Magalhães Paniago, R.; Pimenta, M. A. General Equation for the Determination of the Crystallite Size La of Nanographite by Raman Spectroscopy. *Appl. Phys. Lett.* **2006**, *88*, 163106.

29. Jorio, A.; Martins Ferreira, E. H.; Moutinho, M. V. O.; Stavale, F.; Achete, C. A.; Capaz, R. B. Measuring Disorder in Graphene with the G and D Bands. *Phys. Stat. Sol. B* **2010**, *247*, 2980-2982.

30. Lucchese, M. M.; Stavale, F.; Martins Ferreira, E. H.; Vilani, C.; Moutinho, M. V. O.; Capaz, R. B.; Achete, C. A.; Jorio, A. Quantifying Ion-Induced Defects and Raman Relaxation Length in Graphene. *Carbon* **2010**, *48*, 1592-1597.

31. Martins Ferreira, E. H.; Moutinho, M. V. O.; Stavale, F.; Lucchese, M. M.; Capaz, R. B.; Achete, C. A.; Jorio, A. Evolution of the Raman Spectra from Single-, Few-, and Many-Layer Graphene with Increasing Disorder. *Phys. Rev. B* **2010**, *82*, 125429.

32. Cancado, L. G.; Jorio, A.; Martins Ferreira, E. H.; Stavale, F.; Achete, C. A.; Capaz, R. B.; Moutinho, M. V. O.; Lombardo, A.; Kulmala, T. S.; Ferrari, A. C. Quantifying Defects in Graphene via Raman Spectroscopy at Different Excitation Energies. *Nano Lett.* **2011**, *11*, 3190-3196.

33. Sato, K.; Saito, R.; Oyama, Y.; Jiang, J.; Cancado, L. G.; Pimenta, M. A.; Jorio, A.; Samsonidze, Ge. G.; Dresselhaus, G.; Dresselhaus, M. S. D-Band Raman Intensity of Graphitic Materials as a Function of Laser Energy and Crystallite Size. *Chem. Phys. Lett.* **2006**, *427*, 117–121.

34. Ferrari, A. C.; Basko, D. M. Raman Spectroscopy as a Versatile Tool for Studying the Properties of Graphene. *Nat. Nanotechnol.* **2013**, *8*, 235-246.

35. Vecera, P.; Chacon-Torres, J. C.; Pichler, T.; Reich, S.; Soni, H. R.; Gorling, A.; Edelthalhammer, K.; Peterlik, H.; Hauke, F.; Hirsch, A. Precise Determination of Graphene Functionalization by *in situ* Raman Spectroscopy. *Nat. Comm.* **2017**, *8*, 15192.

36. McGuire, J. A. Growth and Optical Properties of Colloidal Graphene Quantum Dots. *Phys. Stat. Sol. RRL* **2016**, *10*, 91-101.

37. Herziger, F.; Vierck, A.; Laudenbach, J.; Maultzsch, J. Understanding Double-Resonant Raman Scattering in Chiral Carbon Nanotubes: Diameter and Energy Dependence of the D Mode. *Phys. Rev. B* **2015**, *92*, 235409.

38. Laudenbach, J.; Schmid, D.; Herziger, F.; Hennrich, F.; Kappes, M.; Muoth, M.; Haluska, M.; Hof, F.; Backes, C.; Hauke, F.; Hirsch, A.; Maultzsch, J. Diameter Dependence of the Defect-Induced Raman Modes in Functionalized Carbon Nanotubes. Carbon 2017, 112, 1-7.

39. Cancado, L. G.; Pimenta, M. A.; Neves, B. R. A.; Dantas, M. S. S.; Jorio, A. Influence of the Atomic Structure on the Raman Spectra of Graphite Edges. *Phys. Rev. Lett*. **2004**, *93*, 247401.

40. Casiraghi, C.; Hartschuh, A. Qian, H.; Piscanec, S.; Georgi, C.; Fasoli, A.; Novoselov, K. S.; Basko, D. M.; Ferrari, A. C. Raman Spectroscopy of Graphene Edges. *Nano Lett.* **2009**, *9*, 1433-1441.

41. Claramunt, S.; Varea, A.; Lopez-Diaz, D.; Velazquez, M. M.; Cornet, A.; Cirera, A. The Importance of Interbands on the Interpretation of the Raman Spectrum of Graphene Oxide. *J. Phys. Chem. C* **2015**, *119*, 10123-10129.

42. Gupta, A. K.; Russin, T. J.; Gutierrez, H. R.; Eklund, P. C. Probing Graphene Edges via Raman Scattering. *ACS Nano* **2009**, *3*, 45052.

43. Kampmann, F.; Scheuschner, N.; Terres, B.; Jorger, D.; Stampfer, C.; Maultzsch, J. Raman Spectroscopy of Lithographically Defined Graphene Nanoribbons – Influence of Size and Defects. *Ann. Phys*. **2017**, *529*, 1700167.

44. You, Y.; Ni, Z.; Yu, T.; Shen, Z. Edge Chirality Determination of Graphene by Raman Spectroscopy. *Appl. Phys. Lett*. **2008**, *93*, 163112.

45. Casiraghi, C.; Hartschuh, A.; Qian, H.; Piscanec, S.; Georgi, C.; Fasoli, A.; Novoselov, K. S.; Basko, D. M.; Ferrari, A. C. Raman Spectroscopy of Graphene Edges. *Nano Lett*. **2009**, *9*, 1433-1441.

46. Jacobberger, R. M.; Kiraly, B.; Fortin-Deschenes, M.; Levesque, P. L.; McElhinnt, K.; Brady, G. J.; Delgado, R. R.; Roy, S. S.; Mannix, A.; Lagally, M. G.; Evans, P. G.; Desjardins, P.; Martel, R.; Hersam, M. C.; Guisinger, N. P.; Arnold, M. S. Direct Oriented Growth of Armchair Graphene Nanoribbons on Germanium. *Nat. Comm*. **2015**, *6*, 8006.

47. Zhao, S.; Barin, G. B.; Rondin, L.; Raynaud, C.; Fairbrother, A.; Dumslaff, T.; Campidelli, S.; Mullen, K.; Narita, A.; Voisin, C.; Ruffieux, P.; Fasel, R.; Lauret, J.-S. Optical Investigation of On-Surface Synthesized Armchair Graphene Nanoribbons. *Phys. Stat. Sol. B* **2017**, *254*, 1700223.

48. Dervishi, E.; Biris, A. R.; Watanabe, F.; Umwungeri, J. L.; Mustafa, T.; Driver, J. A.; Biris, A. S. Few-Layer Nano-Graphene Structures with Large Surface Areas Synthesized on a Multifunctional Fe:Mo:MgO Catalyst System. *J. Mater. Sci*. **2012**, *47*, 1910-1919.

49. Gillen, R.; Mohr, M.; Thomsen, C.; Maultzsch, J. Vibrational Properties of Graphene Nanoribbons by First-Principle Calculations. *Phys. Rev. B* **2009**, *80*, 155416.

50. Cai, J. M.; Ruffieux, P.; Jaafar, R.; Bieri, M.; Braun, T.; Blankenburg, S.; Muoth, M.; Seitsonen, A. P.; Saleh, M.; Feng, X. L.; Mullen, K.; Fasel, R. Atomically Precise Bottom-Up Fabrication of Graphene Nanoribbons. *Nature* **2010**, *466*, 470-473.

51. Meyer, G. J. Molecular Approaches to Solar Energy Conversion with Coordination Compounds Anchored to Semiconductor Surfaces. *Inorg. Chem*., **2005**, *44*, 6852-6864.

52. Gao, Y.; Roslyak, O.; Dervishi, E.; Karan, N. S.; Ghosh, Y.; Sheehan, C. J.; Wang, F.; Gupta, G.; Mohite, A.; Dattelbaum, A. M.; Doorn, S. K.; Hollingsworth, J. A.; Piryatinski, A.; Htoon, H. Hybrid Graphene-Giant Nanocrystal Quantum Dot Assemblies with Highly Efficient Biexciton Emission. *Adv. Opt. Mater*. **2015**, *3*, 39-43.

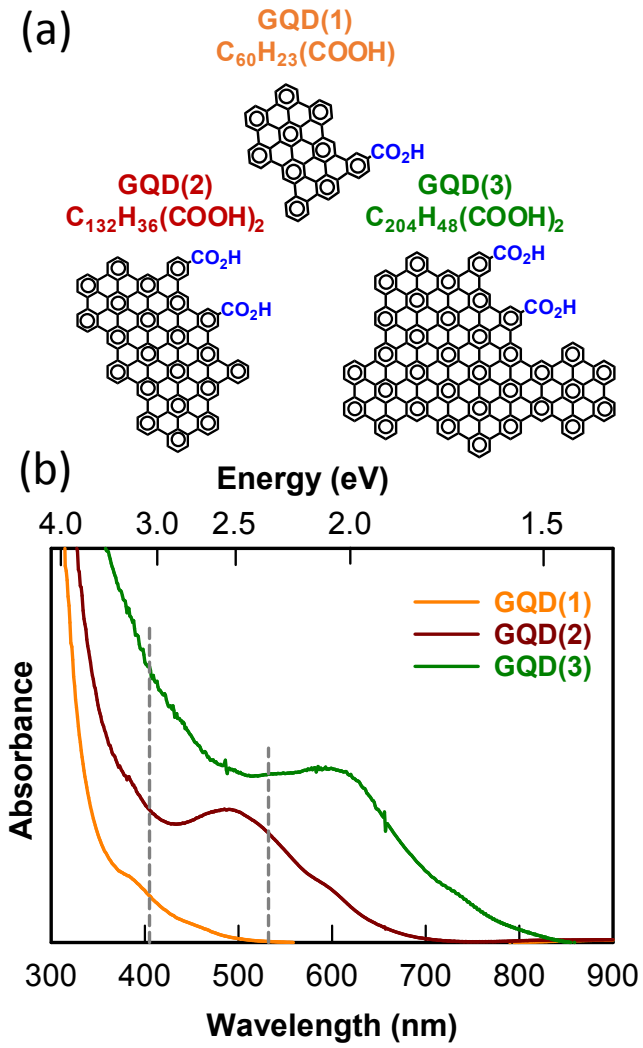

Figure 1. (a) Chemical structures of the GQDs(1-3) with 19, 48 and 79 conjugated rings (60, 132 and 204 conjugated carbon atoms), respectively. (b) UV-Vis-near-IR absorption spectra of the GQDs. The dashed lines indicate the 405 nm and 532 nm excitation wavelengths used for Raman spectroscopy.

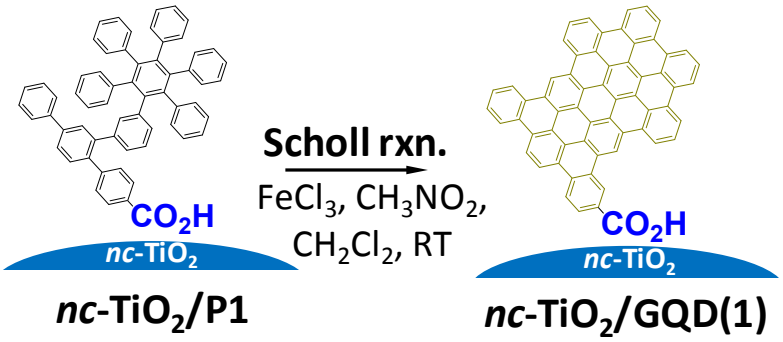

Scheme 1: Schematic depiction of *in-situ* oxidation step leading from *nc*-TiO_2 surface-bound precursor (P1) to final, fully benzenoid GQD(1) structure.

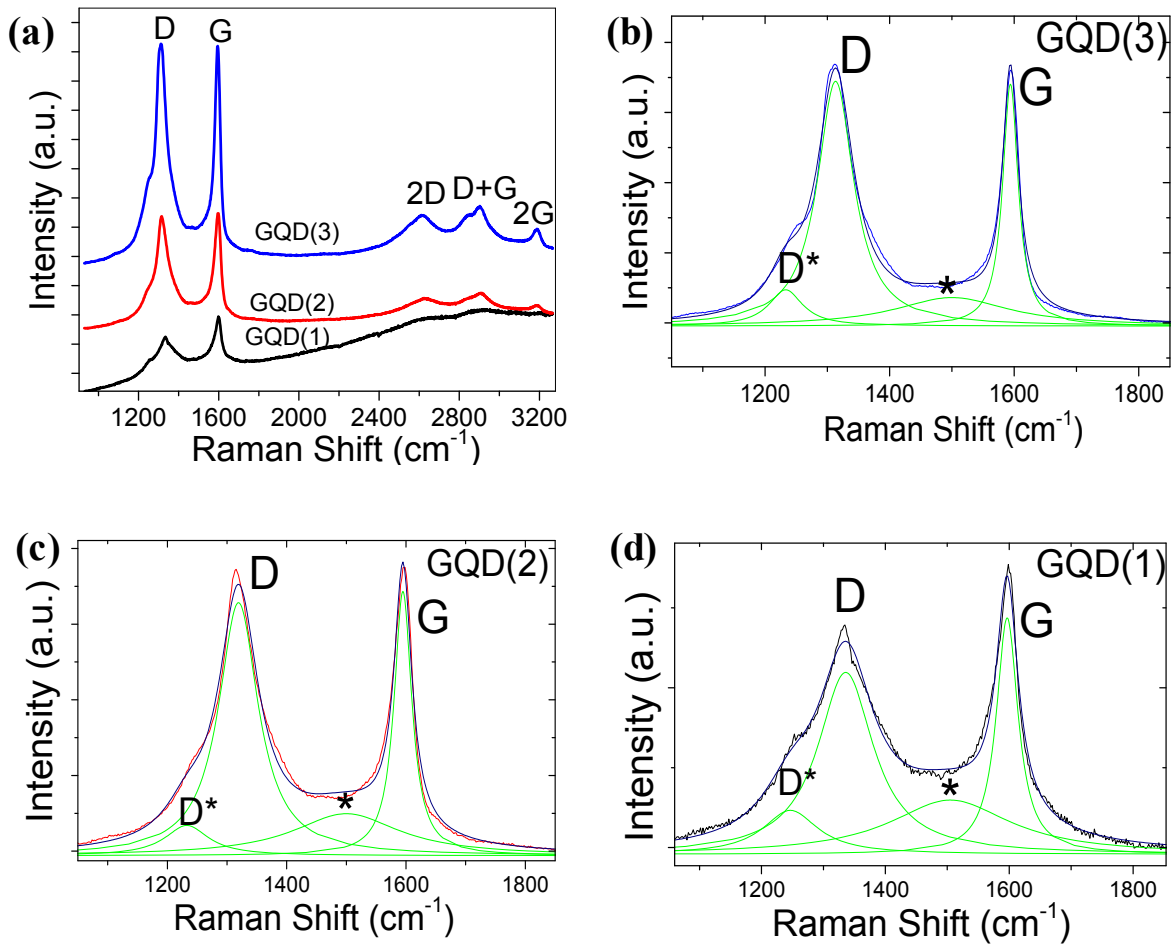

Figure 2. (a) Raman spectra of GQDs (1-3) recorded with 532 nm excitation (spectra are vertically offset for clarity). (b-d) Zoom-in view of the D and G band spectral regions and deconvolution of D and G bands into four Lorentzian components labeled as D*, D, * and G band.

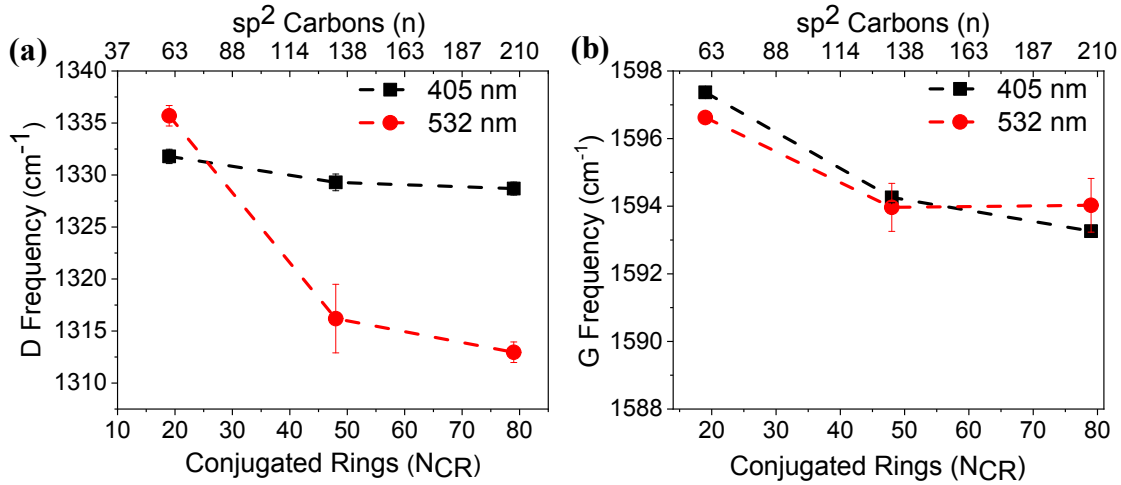

Figure 3: (a) Frequency of D and (b) G bands as a function of GQD size for data taken with 532 nm (red) and 405 nm excitation (black).

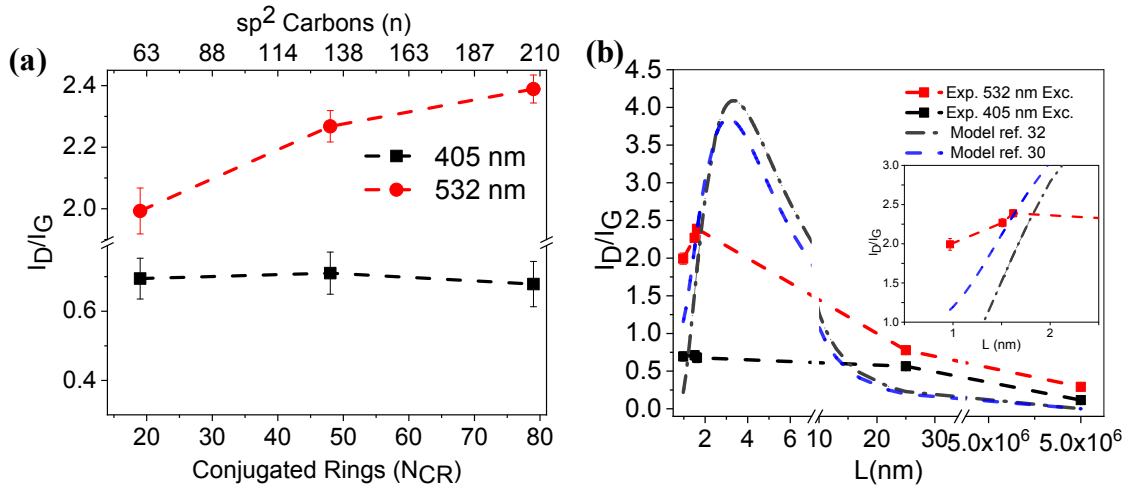

Figure 4: Integrated intensity ratio (I_D/I_G) for D and G-band features as a function of GQD size given as (a) number of ordered rings (N_{CR}) and number of sp2 carbons (n) or (b) average lateral dimension (L), recorded with 405 nm (black) and 532 nm (red) excitation. Superimposed on the experimental data in panel (b) are the results of models from ref. 30 (blue dashed line) and ref. 32 (black dashed line). Inset in (b) is a zoom of the GQD data region.

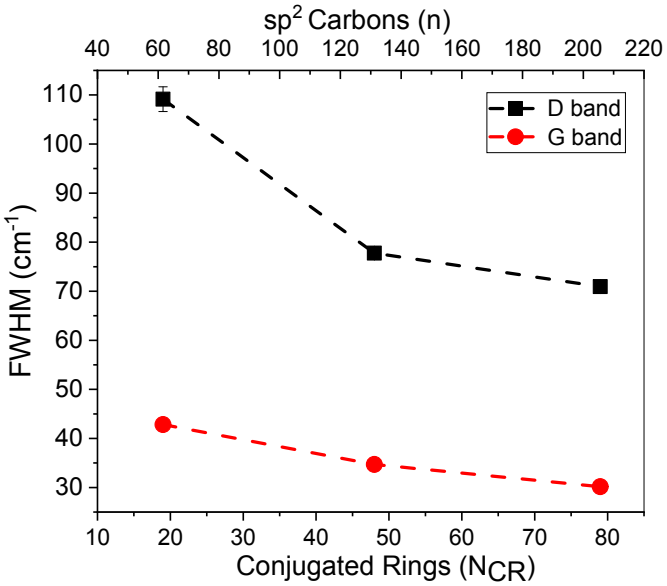

Figure 5. Linewidth (as full width half maximum, FWHM) of D band (black points) and G band (red circles) as a function of GQD size.

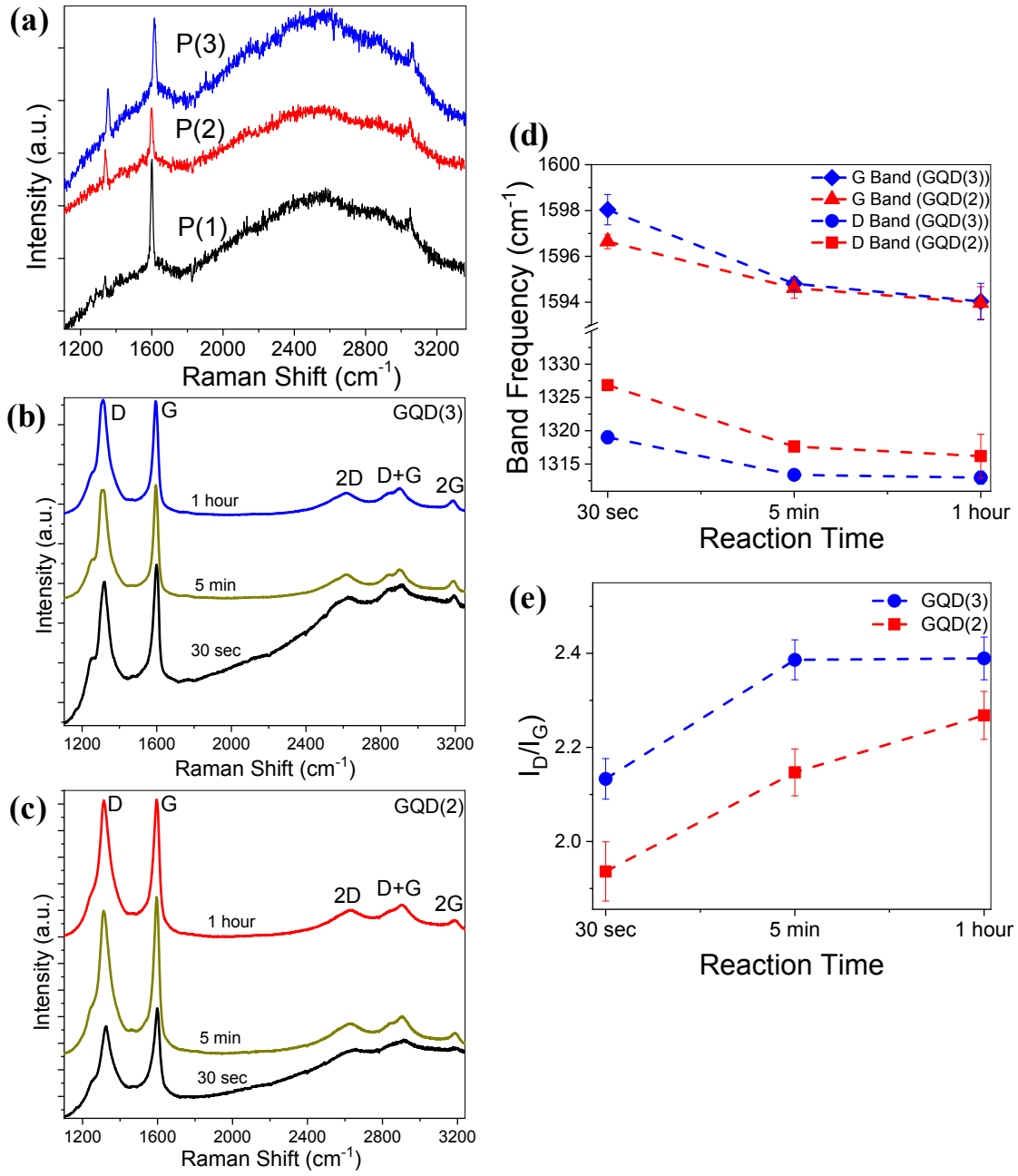

Figure 6: (a) Raman spectra of the GQD precursors. (b, c) Raman spectra of GQD(3) and GQD (2) obtained at different reaction times during synthesis. (Spectra are recorded with 532 nm excitation and vertically offset for clarity.) (d) Integrated intensity ratios (I_D/I_G) as a function of reaction time for GQD(3) and GQD(2). (e) D and G band frequencies as a function of reaction time for GQD(3) and GQD(2).

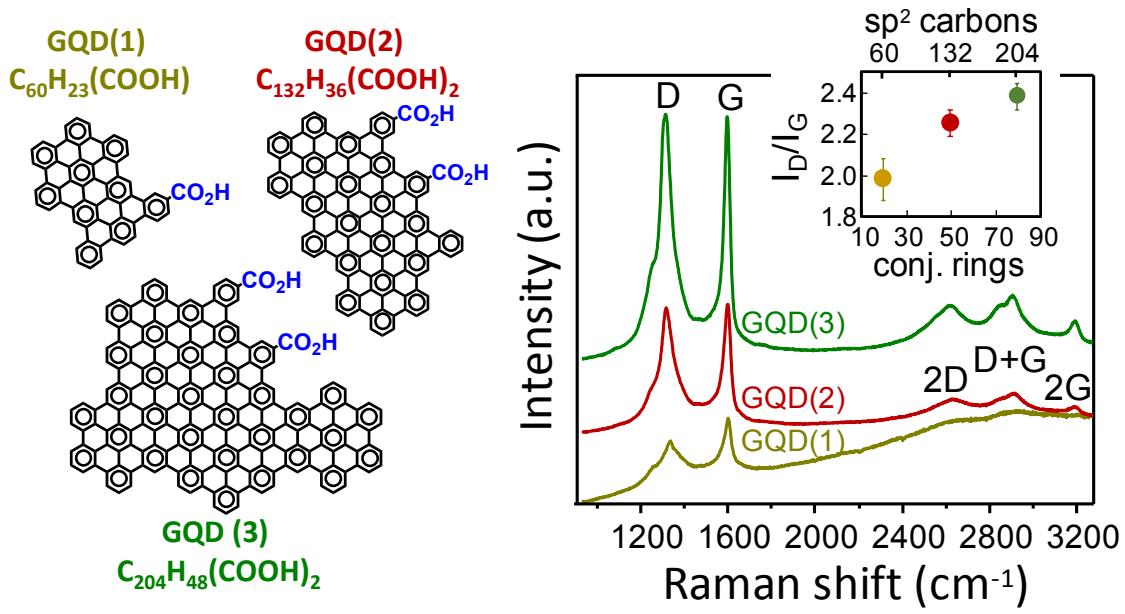

TOC Figure. Dependence of Raman spectra on nanoparticle size was determined for a series of strongly confined graphene quantum dots.